Theor Chem Account (2009) 122:31–42
DOI 10.1007/s00214-008-0482-z

REGULAR ARTICLE

Theoretical studies on electronic structures and spectroscopic properties of a series of novel β-diketonate Os(II) complexes

Jian-Po Zhang · Xin Zhou · Fu-Quan Bai · Hong-Xing Zhang · Au-Chin Tang

Received: 8 July 2008 / Accepted: 12 September 2008 / Published online: 3 October 2008

Abstract The geometries, electronic structures, and spectroscopic properties of a series of $[Os^{(II)}(CO)_3(tfa)(acac(X)_2)]$ (tfa = trifluoroacetate; acac = acetoylacetonate; X = H (**1**), CF_3 (**2**), C_6H_5 (**3**), and $C_{10}H_7$ (**4**)) complexes have been investigated theoretically. The ground and excited state geometries were optimized at the B3LYP/LANL2DZ and CIS/LANL2DZ levels, respectively. The optimized geometry structural parameters agreed well with the corresponding experimental results. As indicated in this paper, the highest occupied molecular orbitals were dominantly localized on the Os atom, ctfa (abbv. of CO and tfa), and acac ligand for **1** and **2**, acac ligand and X substituent for **3** and **4**, while the lowest unoccupied molecular orbitals were mainly composed of acac ligand and X substituent. Under the time-dependent density functional theory (TDDFT) level with the polarized continuum model (PCM), the absorption and phosphorescence in CH_2Cl_2 media were calculated based on the optimized ground- and excited-state geometries, respectively. The calculated results show that the lowest energy absorptions at 317 (**1**), 342 (**2**), 377 (**3**), and 420 nm (**4**) are attributed to a change of ππ*/MLCT mixing transition to pure ππ* transition for **1–4**, while their phosphorescence emission have similar transition properties. This indicates that the absorption and emission transition characters could be altered by adjusting the π electron-donating ability.

Keywords β-Diketonate osmium(II) complexes · Electronic structures · Spectroscopic properties · TD-DFT calculations · CIS methods

1 Introduction

Transition metal complexes of Os(II), possessing heavy transition-metal elements, which are crucial for the fabrication of phosphorescent organic light-emitting diodes (OLEDs) [1–10], have been extensively investigated in the last decades both experimentally and theoretically. The strong spin-orbit coupling effectively promotes singlet-to-triplet intersystem crossing, and enhances the subsequent transition from the triplet-excited state to the ground state, which then facilitates strong electroluminescence by harnessing both singlet and triplet excitons. Theoretically, an internal phosphorescence quantum efficiency (η_{int}) that can be as high as 100% could be achieved [11, 12]. Therefore, these complexes have been widely applied in solar energy conversion, luminescence sensing, biotechnology and electroluminescence displays [13–17].

A series of novel transition metal complexes of β-diketonate, such as (dbm)H, (thd)H, and (acac)H (dbm = dibenzoylmethane, thd = 2,2-dimethyl-3,5-heptanedionate, acac = acetoylacetonate), have received comprehensive attention in recent years [18–23]. These β-diketonate complexes are mainly divided into two types. The first one is formed by the β-diketonate ligand and other bidentate ligands, such as phen(phenanthroline), ppy (phenylpyridine), etc. [20–23]. The other one is formed by the β-diketonate ligand and other monodentate ligands

Electronic supplementary material The online version of this article (doi:10.1007/s00214-008-0482-z) contains supplementary material, which is available to authorized users.

J.-P. Zhang · X. Zhou · F.-Q. Bai · H.-X. Zhang (✉) · A.-C. Tang
State Key Laboratory of Theoretical and Computational Chemistry, Institute of Theoretical Chemistry, Jilin University, Changchun 130023, People's Republic of China
e-mail: zhanghx@jlu.edu.cn; canoe8013@126.com

such as tricarbonyl, halide, and tfa [18, 19]. Several Ir(III) complexes with bidentate ligands such as acac, pico, sal, and dbm (pico = picolinate, sal = *N*-methylsalicylimine) have been synthesized by Thompson and co-workers [21, 24]. The structures, absorption, and emission spectras of these complexes have been studied both theoretically and experimentally. The present results indicate that the lowest-energy absorptions are all assigned to the metal-to-ligand charge transfer (MLCT) transition, because the highest occupied molecular orbitals (HOMO) have larger metal component. This could ensure the high-luminescence efficiency of these complexes. These complexes as phosphors are doped into the emissive layer of the OLEDs, giving a maximum optical output of 32,500 cd/m^2.

Chen et al. have prepared a series complexes of $[Os(CO)_3X((acac)R_1R_2)]$, X = halides or tfa, R_1 or R_2 = $-CF_3$, $-C_6H_5$, $-C_{10}H_7$, etc. [18, 19], based on analogues of fac-$[Re(CO)_3X(L)]$ (X = halides, L = bidentate heterocycles such as 2,2′-bipyridine) complexes [25–31]. Photophysical studies of these Os(II) complexes exhibited low-lying intraligand $\pi\pi^*$ absorptions, prominent $\pi\pi^*$ phosphorescence, unusually long lifetimes and high quantum yields (0.05–0.13). Obviously, the lowest-energy absorptions and emissions of these monodentate complexes are dominated by $\pi\pi^*$ transition; the metals do not play a major role, which is different from the bidentate complexes. Moreover, these $Os(CO)_3$(β-diketonate) fragments have been extensively used as the basic building blocks to construct supramolecular transition–metal complexes, which may serve as model systems for photoresponsive molecular devices [32–35]. For example, the complexes of $[Os_2(CO)_6(thd)_2]$ and $[Os_2(CO)_5(thd)_2]_2$ [36, 37] have been synthesized using hexane solution of (thd)H. So the metal β-diketonate complexes of Os(II) are very important for the developments of material science.

Although there are many experimental studies on the photophysical properties of luminescent β-diketonate Os(II) complexes, there are few corresponding theoretical reports on these complexes. A deep insight into the luminescent mechanism of this kind of complexes is imperative and significant. Therefore, we carried out this work, aimed at providing an in-depth theoretical understanding of the electronic structures and spectroscopic properties of the $[Os(CO)_3(tfa)(acac(X)_2)]$ (X = H (**1**), CF_3 (**2**), C_6H_5 (**3**), and $C_{10}H_7$ (**4**)) complexes, as well as the relationship between the spectra and the X substituent using ab initio and density functional theory (DFT) [38] methods. Significantly, by modifying the peripheral X substituent, the transition properties and phosphorescent color of lowest-energy emissions of these complexes could be tuned, which is very useful for synthesis of new organic luminous materials.

2 Computational details and theory

In this work, Cs symmetry was adopted to set the conformation of these complexes in both the ground and the excited states. The coordination axis is displayed in the Fig. 1. The geometry of the ground state structure is fully optimized by using the density functional theory (DFT) with the B3LYP functional (Becke's three parameter functional and the Lee-Yang-Parr functional) [39], while the geometry of the excited-state structure is fully optimized by the single excitation configuration interaction (CIS) method [40–47]. With such calculations, the spectroscopic properties related to absorption and emission are obtained by the time dependent density functional theory (TD-DFT) [48–50] at B3LYP functional associated with the polarized continuum model (PCM) [51, 52]. This kind of theoretical approach has been proven to be reliable for transition metal complex systems [53, 54]. In order to simulate the UV–visible spectra, the 40 lowest spin-allowed singlet transitions are investigated.

In the calculations, quasirelativistic pseudopotentials of the Os atoms proposed by Hay [55] and Wadt [56] with 16 valence electrons were employed, and the LANL2DZ basis sets associated with the pseudopotential were adopted. To describe the molecular properties precisely one additional f-type function was implemented for Os (α = 0.886). The basis sets were described as Os (8s6p3d1f|3s3p2d1f), C, O, F (10s5p|3s2p), and H (4s|2s). Therefore, 197 basis functions and 150 electrons for **1**, 265 basis functions and 214 electrons for **2**, 321 basis functions and 230 electrons for **3**, 401 basis functions and 282 electrons for **4** are included in the calculations. All the calculations are accomplished by using the Gaussian03 (Revision C.02) program package [57] on an origin/3900 server.

3 Results and discussion

3.1 The geometries and frequencies of the four complexes in the ground and excited states

The geometry of the structure is depicted in Fig. 1, and the main optimized geometry parameters of these complexes in the ground and excited states are listed in Table 1, together with the X-ray crystal structure data of analogues $[Os(CO)_3I(dbm)]$ (dbm = dibenzoylmethane) [19]. These complexes have a $^1A'$ ground state and an $^3A'$ excited state. As shown in Fig. 1, the atoms of Os, O(4), C(1), and O(1) pass through the symmetric plane.

From Table 1, the optimized bond lengths of **1**–**4** in the ground state are in general agreement with the available X-ray data. The calculated bond distances of Os–C(1) (1.891 Å), and Os–C(2) (1.916 Å) are ca. 0.03 and

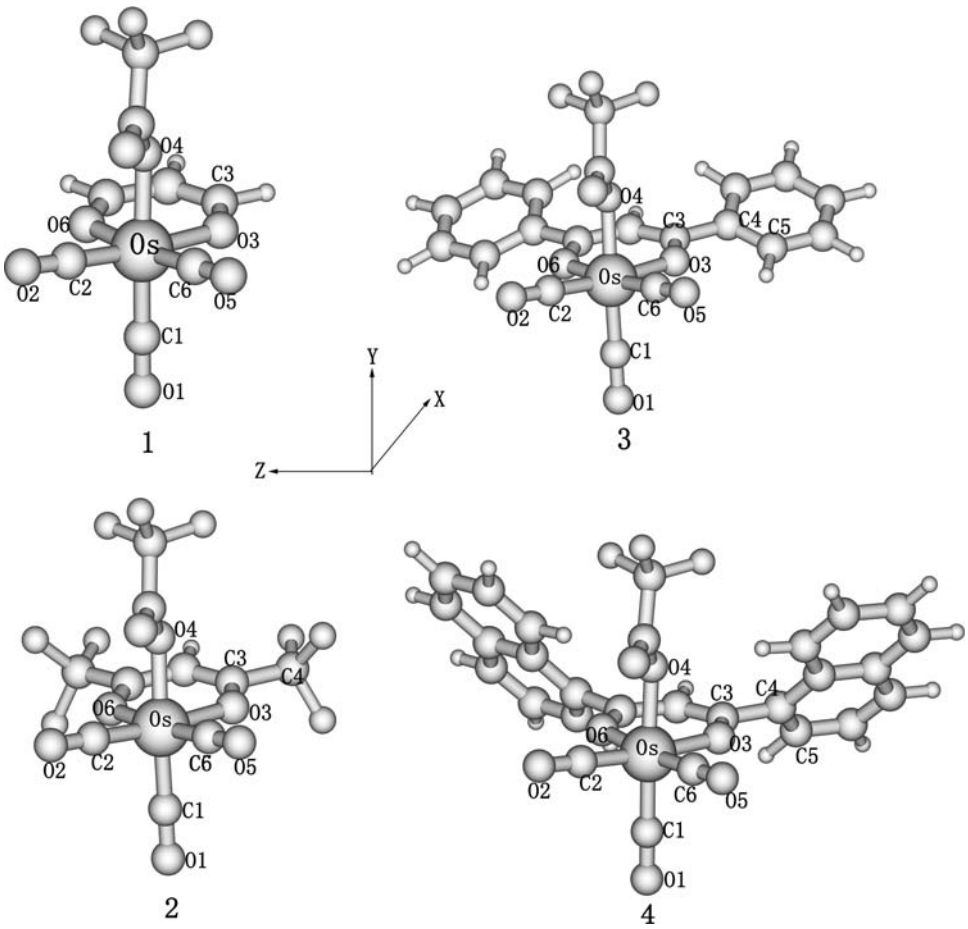

Fig. 1 Optimized geometry structures of **1–4** at the B3LYP/LANL2DZ level

Table 1 Main optimized geometry structural parameters of the complexes in the ground and lower lying triplet excited states at the B3LYP and CIS levels, respectively, together with the experimental values

Parameter	1		2		3		4		Expt[a]
	$^1A'$	$^3A'$	$^1A'$	$^3A'$	$^1A'$	$^3A'$	$^1A'$	$^3A'$	
Bond lengths (Å)									
Os–C(1)	1.910	1.956	1.911	1.968	1.891	1.951	1.905	1.950	1.928
Os–C(2)	1.912	1.955	1.914	1.957	1.916	1.957	1.913	1.963	1.917
Os–O(3)	2.092	2.076	2.097	2.088	2.093	2.081	2.092	2.082	2.088
Os–O(4)	2.066	2.040	2.058	2.028	2.072	2.039	2.074	2.037	
C(1)–O(1)	1.168	1.133	1.166	1.131	1.172	1.134	1.169	1.134	
C(2)–O(2)	1.165	1.132	1.163	1.130	1.168	1.133	1.166	1.131	
Bond angles (°)									
O(3)–Os–O(6)	87.9	85.6	86.0	83.1	86.8	83.9	87.0	85.0	
C(2)–Os–O(3)	175.2	173.9	174.9	173.1	174.7	174.1	175.1	174.4	
C(1)–Os–O(4)	171.0	169.9	170.6	169.3	170.9	170.2	171.5	170.8	
Dihedral angles (°)									
C(3)–O(3)–Os–O(4)	−72.4	−65.6	−69.2	−60.9	−70.6	−63.2	−79.6	−78.3	
O(3)–C(3)–C(4)–C(5)					158.6	173.2	135.6	140.5	

[a] From Ref. [19]

0.001 Å, compared with the corresponding analogues experimental values, respectively. The average osmium–carbon bond distance (1.900 Å) is shorter than that of the sum (2.04 Å) of the covalent radii of Os and sp- and sp^3-hybridized carbons [58, 59]. These structural data indicate significantly π conjugation among the metal-carbonyl moieties. The bond distance of Os–O(3) (2.093 Å) is overestimated by about 0.01 Å. In addition, the bond angles and dihedral angles are also reproduced. The bond angles of C(2)–Os–O(3) of **1–4** is about 175.0°. The dihedral angle of O(3)–C(3)–C(4)–C(5) is 158.6° for **3**, and 135.6° for **4**; it is in favor of forming the π-conjugation between the acac ligand and X substituents. Therefore, X substituents would act as a strong electron donator in complexes **3** and **4** when needed. The discrepancy of the dihedral angle between **3** and **4** is reasonable and acceptable, since the effect of steric hindrance is bigger for **4**.

The main geometry structural parameters of the complexes in the $^3A'$ excited states obtained by the CIS method are given in Table 1. The geometry parameters of lowest-lying triplet excited state of **1–4**, which show similar tendency, are slightly different from their ground state. The calculated Os–C(1) and Os–C(2) bond lengths relax by 0.04–0.06 Å, but the Os–O(3) and Os–O(4) bond lengths strengthen by 0.02–0.04 Å. The calculated O(3)–Os–O(6) bond angle reduces by 2.0°–3.0°. The slight changes of the geometry structural parameters result from the electron transfer from the carbonyl ligand to the acac ligand, which enhance the interaction between Os(II) atom and acac ligand, and weaken the interaction between Os(II) atom and carbonyl ligand upon excitation.

The frequencies of **1–4** in the ground and excited states are calculated, and the calculation results for C=O, Os–C(1), Os–C(2), Os–O(3), and Os–O(4) stretching mode are shown in Table 2. From Table 2, we can see the υ(C=O) stretching frequency in the ground state appears at 2,118, 2,063, and 1,983 cm^{-1} for **3**, which is in good agreement with the experimental data of 2,125, 2,047, and 2,031 cm^{-1} [19]. Moreover, other complexes also have three analogous stretching frequencies. The υ(C=O) stretching frequency in the $^3A'$ excited state appears at 2,291, 2,226, and 2,223 cm^{-1} for **3**, the enhancement of the C=O stretching frequency in the excited state indicates the strengthening of the C=O bonding interaction, which is consistent with the shortening of the C=O bond distance in the excited state. The change trend of the υ(Os–O(3)) and υ(Os–O(4)) is similar to that of υ(C=O) (see Table 2). In contrast, the Os–C(1) and Os–C(2) stretching frequencies reduced in the excited state relative to their ground state, being in line with the lengthening of their bond lengths in the excited state. There have also been similar vibration characteristics of $[OsN(C\equiv CH)_4]$ [60] and $Ir(C\text{^}N)_2LX$ [23] (C^N = bzq, LX = acac, bzq = benzoquinoline, acac = acetoylacetonate) complexes, the enhancement of stretching frequency along with the bond length shortening from ground state to excited state, and vice versa.

3.2 Electronic structure and absorptions spectra of **1–4** in the ground states

Frontier molecular orbitals, in particular the HOMO and lowest unoccupied molecular orbitals (LUMO) are very important, which are related to photoelectronic spectra and UV spectra. A detailed analysis of the frontier molecular orbital compositions and energies of these complexes is presented in Tables 3, 4, 5, and 6, respectively. Moreover, in order to intuitively understand the orbital and transition processes, we display the schematic representation of energies and related transitions of some frontier MO for these complexes in Fig. 2.

Some interesting trends in the frontier molecular orbital components and energies of **1–4** are summarized as follows:

(1) The components of HOMO of **1–4** come mainly from d(Os), π(ctfa), π(acac), and π(X) orbitals, while the LUMO come mainly from π*(acac), and π*(X) orbitals.

Table 2 The calculated and experiment frequency values of the C=O, Os–C, and Os–O stretching modes in the ground and excited states of **1–4** under B3LYP calculations

Frequency (cm^{-1})	1		2		3		4		Expt[a]
	$^1A'$	$^3A'$	$^1A'$	$^3A'$	$^1A'$	$^3A'$	$^1A'$	$^3A'$	
υ(C=O) A	2,083	2,295	2,093	2,306	2,118	2,291	2,077	2,297	2,125
υ(C=O) B	2,013	2,234	2,026	2,248	2,063	2,226	2,005	2,226	2,047
υ(C=O) C	1,997	2,226	2,010	2,240	1,983	2,223	1,993	2,225	2,031
υ(Os–C(1))	509	462	508	426	518	442	511	441	
υ(Os–C(2))	484	439	482	413	486	428	488	421	
υ(Os–O(3))	584	594	590	601	581	589	606	611	
υ(Os–O(4))	617	625	620	628	612	625	614	624	

[a] From Ref. [19]

Table 3 Molecular orbital compositions in the ground state for $[Os(CO)_3(tfa)(acac(H)_2)]$ (**1**) at the B3LYP level

Orbial	Energy (ev)	Composition (%)			Main bond type	Os comp.
		Os	ctfa	acac		
54a′	−0.7603	24.9	72.4		d(Os) + π*(ctfa)	$19.6d_{yz}$
53a′	−0.9344	23.3	74.0		d(Os) + π*(ctfa)	$11.9d_{xy}$
29a″	−1.2422		96.0		π*(ctfa)	
52a′	−1.3451	29.4	64.2		d(Os) + π*(ctfa)	$9.6d_{xy} + d_{x^2-y^2}$
28a″	−1.4637		98.7		π*(ctfa)	
51a′	−2.1133	17.3	74.2		d(Os) + π*(ctfa)	
27a″	−2.1402	13.1	58.7	28.3	d(Os) + π*(ctfa) + π*(acac)	
50a′	−2.3783		19.0	74.7	π*(acac) + π*(ctfa)	
HOMO–LUMO energy gap						
49a′	−7.0448	13.6	11.1	75.3	d(Os) + π(acac) + π(ctfa)	$7.0d_{z^2}$
26a″	−8.0203	44.8	51.6		d(Os) + π(ctfa)	$35.5d_{yz}$
25a″	−8.0628	45.3	27.9	26.9	d(Os) + π(ctfa) + π(acac)	$26.6d_{x^2-y^2} + 10.1d_{z^2}$
48a′	−8.3945		83.6		π(ctfa)	
47a′	−8.4699		14.7	79.4	π(dbm) + π(ctfa)	
24a″	−8.7112	53.5	36.2	10.4	d(Os) + π(ctfa) + π(dbm)	$41.7d_{xy} + d_{yz}$
23a″	−9.3077	21.7	62.1	16.3	d(Os) + π(ctfa) + π(dbm)	$17.5d_{yz}$

Table 4 Molecular orbital compositions in the ground state for $[Os(CO)_3(tfa)(acac(CF_3)_2)]$ (**2**) at the B3LYP level

Orbital	Energy (ev)	Composition (%)				Main bond type	Os comp.
		Os	ctfa	acac	CF_3		
68a′	−1.2302	22.6	75.0			d(Os) + π*(ctfa)	$15.9d_{xy}$
46a″	−1.4017		94.6			π*(ctfa)	
45a″	−1.6490		98.7			π*(ctfa)	
67a′	−1.6504	29.0	64.1			d(Os) + π*(ctfa)	$12.7d_{x^2-y^2}$
66a′	−2.4120	19.1	70.4			d(Os) + π*(ctfa)	
44a″	−2.5040	20.0	61.4	16.3		d(Os) + π(ctfa) + π*(acac)	$5.5d_{xz} + 4.7d_{z^2}$
43a″	−3.7046			79.6	15.3	π*(acac) + π*(CF_3)	
HOMO–LUMO energy gap							
65a′	−7.8331	21.9	15.6	61.1		d(Os) + π(acac) + π(ctfa)	$9.3d_{z^2}$
42a″	−8.2478	38.6	58.9			d(Os) + π(ctfa)	$25.6d_{xz}$
64a′	−8.3436	13.7	82.2			d(Os) + π(ctfa)	
63a′	−8.6753	44.0	31.6	22.9		d(Os) + π(ctfa) + π(acac)	$26.8d_{yz}$
62a′	−9.1752	45.6	32.3	20.8		d(Os) + π(ctfa) + π(acac)	$22.6d_{xy} + 14.6d_{x^2-y^2}$
41a″	−9.4242	11.8	23.1	50.2	14.9	d(Os) + π(ctfa) + π(acac) + π(CF_3)	
40a″	−9.6555	20.6	37.7	32.4	9.3	d(Os) + π(acac) + π(ctfa) + π(CF_3)	$15.5d_{xz}$

The compositions of the metal in HOMO are decreased, but the compositions of the X substituent in HOMO and LUMO are increased with the increasing of the π electron-donating abilities in the order of CF_3 (**2**) < H (**1**) < C_6H_5 (**3**) < $C_{10}H_7$ (**4**). So the metal-to-ligand charge transfer (MLCT) transition is decreased, and ligand-to-ligand/intraligand charge transfers (LLCT/ILCT) transition are increased from **2** to **1**, **3** and **4**. In addition, the effect of X substituents for NHOMO (next HOMO) orbitals components is bigger compared with NLUMO, especially for **3** and **4**.

(2) The energy levels of the HOMO increase in the order of **2** < **1** < **3** < **4**, which is consistent with the increasing trend of the π electron-donating ability of X substituents in the order of CF_3 < H < C_6H_5 < $C_{10}H_7$, while the energy levels of the LUMO of the substituted derivatives (**2–4**)

Table 5 Molecular orbital compositions in the ground state for $[Os(CO)_3(tfa)(acac(C_6H_5)_2)]$ (**3**) at the B3LYP level

Orbital	Energy (ev)	Composition (%)				Main bond type	Os comp.
		Os	ctfa	acac	C_6H_5		
73a′	−0.7821		20.6	13.4	57.6	$\pi^*(C_6H_5) + \pi^*(ctfa) + \pi^*(acac)$	
72A′	−0.9402	17.9	58.2		16.3	$d(Os) + \pi^*(ctfa) + \pi^*(C_6H_5)$	$9.6d_{z^2}$
50a″	−1.1723		96.5			$\pi^*(ctfa)$	
71a′	−1.2803	28.9	63.1			$d(Os) + \pi^*(ctfa)$	$14.8d_{xy}$
49a″	−1.3924		97.7			$\pi^*(ctfa)$	
48a″	−2.1356	16.6	65.1	14.7		$d(Os) + \pi^*(ctfa) + \pi^*(acac)$	$4.6d_{xy}$
70a′	−2.1388	16.5	73.1			$d(Os) + \pi^*(ctfa)$	$6.9d_{z^2}$
47a″	−2.6629			60.7	32.5	$\pi^*(acac) + \pi^*(C_6H_5)$	
HOMO–LUMO energy gap							
69a′	−6.5730	3.9		55.1	36.8	$\pi(acac) + \pi(C_6H_5)$	$1.5d_{x^2-y^2}$
46a″	−7.1967				91.5	$\pi(C_6H_5)$	
68a′	−7.2048				94.2	$\pi(C_6H_5)$	
45a″	−7.2845			14.8	72.5	$\pi(C_6H_5) + \pi(acac)$	
67a′	−7.4059	18.6	12.4	30.9	38.2	$d(Os) + \pi(C_6H_5) + \pi(acac) + \pi(ctfa)$	$7.9d_{xy}$
66a′	−7.9167	42.2	19.1	32.5		$d(Os) + \pi(acac) + \pi(ctfa)$	$23.1d_{yz}$
44a″	−8.0867	38.3	53.1			$d(Os) + \pi(ctfa)$	$30.2d_{xz}$
65a′	−8.3504		91.6			$\pi(ctfa)$	
43a″	−8.4367		12.6	63.4	19.3	$\pi(acac) + \pi(C_6H_5) + \pi(ctfa)$	
64a′	−8.7809	49.2	31.9	12.2		$d(Os) + \pi(ctfa) + \pi(acac)$	$36.3d_{xy}$

Table 6 Molecular orbital compositions in the ground state for $[Os(CO)_3(tfa)(acac(C_{10}H_7)_2)]$ (**4**) at the B3LYP level

Orbital	Energy (ev)	Composition (%)				Main bond type	Os comp.
		Os	ctfa	acac	$C_{10}H_7$		
84a′	−1.3772	10.5	20.9	10.3	58.3	$d(Os) + \pi^*(C_{10}H_7) + \pi^*(ctfa) + \pi^*(acac)$	$5.4d_{x^2-y^2}$
83a′	−2.0629	16.7	73.4			$d(Os) + \pi^*(ctfa)$	$6.1d_{z^2}$
61a″	−2.0918	15.7	64.3	15.7		$d(Os) + \pi^*(ctfa) + \pi^*(acac)$	
60a″	−2.5084			57.1	35.0	$\pi^*(acac) + \pi^*(C_{10}H_7)$	
HOMO–LUMO energy gap							
82a′	−6.0304	0.2		9.4	90.2	$\pi(C_{10}H_7) + \pi(acac)$	
59a″	−6.1087				91.1	$\pi(C_{10}H_7)$	
81a′	−6.8467			25.6	66.6	$\pi(C_{10}H_7) + \pi(acac)$	
58a″	−6.8668				98.2	$\pi(C_{10}H_7)$	
80a′	−6.9126	9.0		49.3	34.8	$d(Os) + \pi(acac) + \pi(C_{10}H_7)$	$3.9d_{x^2-y^2}$
79a′	−7.7782	36.8	16.1	31.4	15.7	$d(Os) + \pi(acac) + \pi(ctfa) + \pi(C_{10}H_7)$	$20.9d_{yz}$
57a″	−7.8299	33.9	30.6		29.0	$d(Os) + \pi(ctfa) + \pi(C_{10}H_7)$	$25.7d_{xz}$
78a′	−7.9874	22.7	18.1	13.7	45.5	$d(Os) + \pi(C_{10}H_7) + \pi(ctfa) + \pi(acac)$	$10.1d_{yz} + 7.0d_{z^2}$
56a″	−7.9880	13.9	30.0	15.2	40.8	$d(Os) + \pi(C_{10}H_7) + \pi(ctfa) + \pi(acac)$	$9.8d_{xz}$

decreased compared with their parent complex **1**. So, apparently the energy gaps of HOMO–LUMO of **3** and **4** shrank, compared with that of **1**. Moreover, for **2** the decreasing of energy level of the LUMO is more remarkable than that of HOMO, resulting in narrowing of HOMO–LUMO energy gaps. Therefore, we conclude that the wavelengths of the electronic ground bands of **2–4** are red-shifted, compared with its parent complex **1**. And, the change trend of orbital energy of NHOMO and NLUMO is in agreement with their HOMO and LUMO.

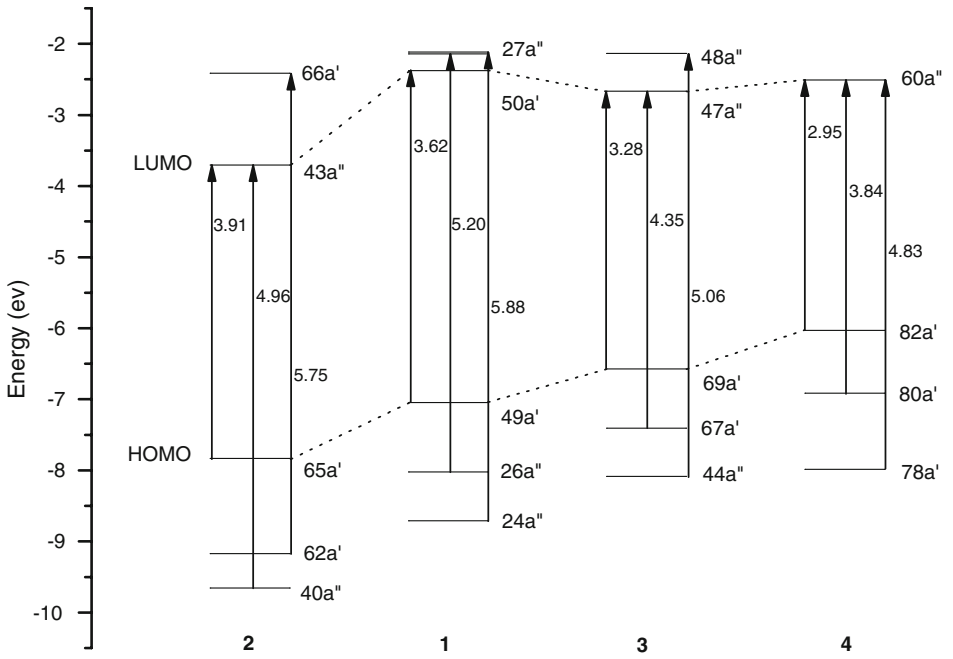

Fig. 2 Schematic representation of energies and related energy transitions of some frontier MO in four complexes

According to the vertical electron transition mechanism in the absorption process, the optimized ground-state geometry of the complexes is kept upon the calculation of the electron transition. Within the considered energy range, the absorption spectra of **1–4** show three absorption bands, the most representative optical transitions and their oscillator strengths, the main configurations, their assignments, the absorptions of acac$(X)_2^-$ ligand, and the experimental results [19] as given in Table 7. The fitted Gaussian type absorption curves are shown in Fig. 3. To intuitively understand the transition process, we display the electron density diagrams in Figs. 4, S1, and S2 (Supporting Information).

For the lowest-lying distinguishable absorption bands, the most representative absorption of **1–4** is at 317 (3.71 eV), 342 (3.62 eV), 377 (3.28 eV), and 420 nm (2.95 eV), respectively. Table 7 shows that the excitation of MO 49a′ → MO 50a′ with the largest CI coefficient of 0.52 dominates the absorption of **1**. Based upon the above discussion on the frontier molecular orbitals, this absorption can be described as a [d(Os) + π(acac) + π(ctfa)] → [π*(acac) + π*(ctfa)] transition with LLCT/ILCT/MLCT character, while the lowest energy absorption band of **2** at 342 nm has a similar transition path. But for **3**, the excitation of MO 69a′ → MO 47a″ (CI = 0.67) is responsible for the absorption at 377 nm. As seen in Table 5, MO 69a′ (HOMO) composed of about 36.8% C_6H_5 substituent and 55.1% acac ligand, while the MO 47a″ (LUMO) lies above the HOMO by about 3.9 eV, is mainly localized on the acac ligand and C_6H_5 substituent. Therefore, the absorption of **3** at 377 nm is assigned to [π(acac) + π(C_6H_5)] → [π*(acac) + π*(C_6H_5)] transition with C_6H_5-to-acac ligand charge transfer (XLCT) and intraligand charge transfer (ILCT) character, while the transition character of **4** at 420 nm is similar to that of **3** at 377 nm. To intuitively understand the absorption of **1**–**4**, we display the electron density diagrams in Fig. 4, in which four single electron excitations corresponding to the maximal CI coefficients are involved. With respect to the absorptions of **2** at 342 nm, the electron density diagram shows that the charge transfer located on the Os, acac ligand, and CF_3 substituent is attributed to ππ*/MLCT characters, which are in accordance with transition character of **2** at 336 nm experimentally.

By comparing the absorptions of **2–4** at 342, 377, and 420 nm, we find that the lowest-lying absorptions of the substituent complexes **2–4** are red-shift, according to increasing trend of the π electron-donating ability of X substituting group in the order of $–CF_3 < –C_6H_5 < –C_{10}H_7$. Moreover, for the lowest-energy absorptions of **3** and **4**, the oscillator strength of 0.77 and 0.59 is far larger than that of corresponding lowest-energy absorptions of **1** and **2**. The phenomenon can be attributed to the presence of the strong resonance forms when strong electron-donating group are attached to the acac ligand, namely, the spin-allowed lowest-lying absorptions band, undergoes an increase of intensity and a red shift, regardless of the electron-donor or electron-acceptor nature of the substituents. In addition, we have calculated the lowest-energy absorption of (acac)$(C_{10}H_7)_2^-$ ligand at 393.79 nm, which is close to the lowest-energy absorption of **4** at 420 nm. This indicates that the contribution of metal Os to the lowest-energy absorption

Table 7 Absorptions and phosphorescence of **1–4** in CH_2Cl_2 under TD-DFT (B3LYP) calculations, together with experimental values

	Transition	Config (CI coeff)	E, nm (ev)	Oscillator	Assignment	λ_{exptl} (nm)[a]
Absorptions						
1	$X^1A \rightarrow A^1A''$	$49a' \rightarrow 50a'$ (0.52)	317.47 (3.91)	0.0146	LLCT/ILCT/MLCT	
		$49a' \rightarrow 27a''$ (0.45)				
	$X^1A \rightarrow B^1A'$	$26a'' \rightarrow 27a''$ (0.58)	250.19 (4.96)	0.0789	MLCT/LLCT	
	$X^1A \rightarrow C^1A'$	$24a'' \rightarrow 51a'$ (0.35)	215.79 (5.75)	0.1219	MLCT/LLCT	
		$26a'' \rightarrow 28a''$ (0.34)				
2	$X^1A \rightarrow A^1A''$	$65a' \rightarrow 43a''$ (0.59)	342.72 (3.62)	0.0288	LXCT/ILCT/MLCT	336
	$X^1A \rightarrow B^1A''$	$40a'' \rightarrow 43a''$ (0.55)	238.35 (5.20)	0.0784	MLCT/LLCT	
	$X^1A \rightarrow C^1A'$	$62a' \rightarrow 66a'$ (0.36)	210.89 (5.88)	0.0238	MLCT/LLCT	
		$65a' \rightarrow 68a'$ (0.24)				
3	$X^1A \rightarrow A^1A''$	$69a' \rightarrow 47a''$ (0.67)	377.84 (3.28)	0.7719	XLCT/ILCT	367
	$X^1A \rightarrow B^1A''$	$67a' \rightarrow 47a''$ (0.55)	284.95 (4.35)	0.0539	MLCT/LLCT	280
	$X^1A \rightarrow C^1A'$	$44a'' \rightarrow 48a''$ (0.59)	245.16 (5.06)	0.0459	MLCT/LLCT	
4	$X^1A \rightarrow A^1A''$	$82a' \rightarrow 60a''$ (0.69)	420.61 (2.95)	0.5880	XLCT/ILCT	
	$X^1A \rightarrow B^1A''$	$80a' \rightarrow 60a''$ (0.56)	322.56 (3.84)	0.0526	MLCT/LLCT	
	$X^1A \rightarrow C^1A''$	$78a' \rightarrow 60a''$ (0.47)	256.60 (4.83)	0.1579	MLCT/LLCT	
Ligand($acac(X)_2$) Absorptions						
1	$X^1A \rightarrow A^1B_2$	$2b_1 \rightarrow 2a_2$ (0.60)	246.89 (5.02)	0.4389	$\pi \rightarrow \pi^*$	
2	$X^1A \rightarrow A^1B_2$	$3b_1 \rightarrow 3a_2$ (0.61)	249.21 (4.98)	0.4371	$\pi \rightarrow \pi^*$	
3	$X^1A \rightarrow A^1B_2$	$10b_1 \rightarrow 11a_2$ (0.54)	256.54 (4.82)	0.5245	$\pi \rightarrow \pi^*$	
4	$X^1A \rightarrow A^1A''$	$44a' \rightarrow 42a''$ (0.66)	393.79 (3.15)	0.2689	$\pi \rightarrow \pi^*$	
Phosphorescences						
1	$X\ ^3A \rightarrow A\ ^1A'$	$27a'' \rightarrow 49a'$ (0.56)	444.41 (2.79)		^{3}LLCT/^{3}ILCT/^{3}MLCT	
		$50a' \rightarrow 49a'$ (0.50)				
2	$X^3A \rightarrow A^1A'$	$43a'' \rightarrow 65a'$ (0.75)	521.54 (2.38)		^{3}LLCT/^{3}LXCT/^{3}MLCT	545
3	$X^3A \rightarrow A^1A'$	$47a'' \rightarrow 69a'$ (0.75)	561.15 (2.21)		^{3}LXCT/^{3}ILCT	541
4	$X^3A \rightarrow A^1A'$	$60a'' \rightarrow 82a'$ (0.61)	525.48 (2.36)		^{3}XLCT/^{3}ILCT	

[a] From Refs. [18, 19]

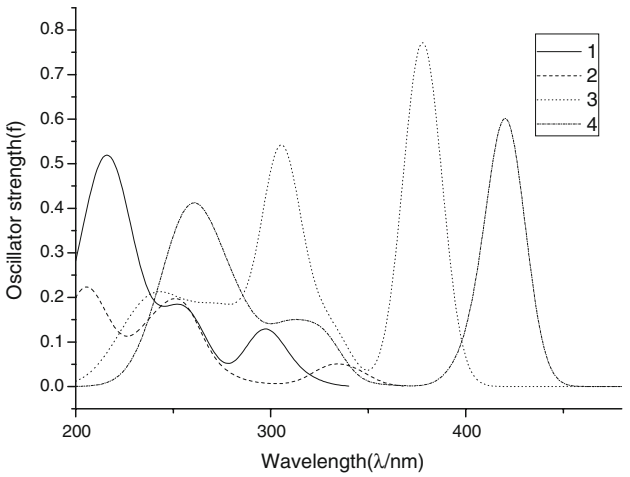

Fig. 3 Simulated absorption spectra with Gaussian curve based on the data calculated under the TD-DFT method in CH2CL2 for **1–4**

is very small and the lowest-energy absorption is from $\pi\pi^*$ transition, which are in accordance with the analysis of the frontier molecular orbital compositions.

Table 7 shows that the most representative absorption of second absorption band of **1–4** are at 250 (4.96 eV), 238 (5.20 eV), 284 (3.28 eV), and 322 (3.84 ev), respectively. With respect to **1**, the excitation of MO $26a'' \rightarrow$ MO $27a''$ with the configuration coefficient of 0.58 contributes to the absorption at 250 nm. Table 3 shows that MO $26a''$ has 35.5% d_{yz}(Os), and 51.6% π(ctfa), while MO $27a''$ has 13.1% d(Os), 58.7% π(ctfa), and 28.3% π(acac) composition. Thus the absorption at 250 nm is mainly attributed to a [d_{yz}(Os) + π(ctfa)] $\rightarrow$ [π^*(ctfa) + π^*(acac)] transition with MLCT/LLCT character, while the absorption of **2-4** at 238, 284, and 322 nm has similar transition character to that of **1** at 250 nm, except for the slight effect of X substituent. By the second absorption band, we find that with the increasing of π electron-donating ability of X substituent in the order of **2** < **1** < **3** < **4**, the absorption wavelengths are red-shifted, which is different from the first absorption band. From the electronic density diagrams depicted in Fig. S1, the absorptions of **2** and **3** are assigned to the MLCT/$\pi\pi^*$

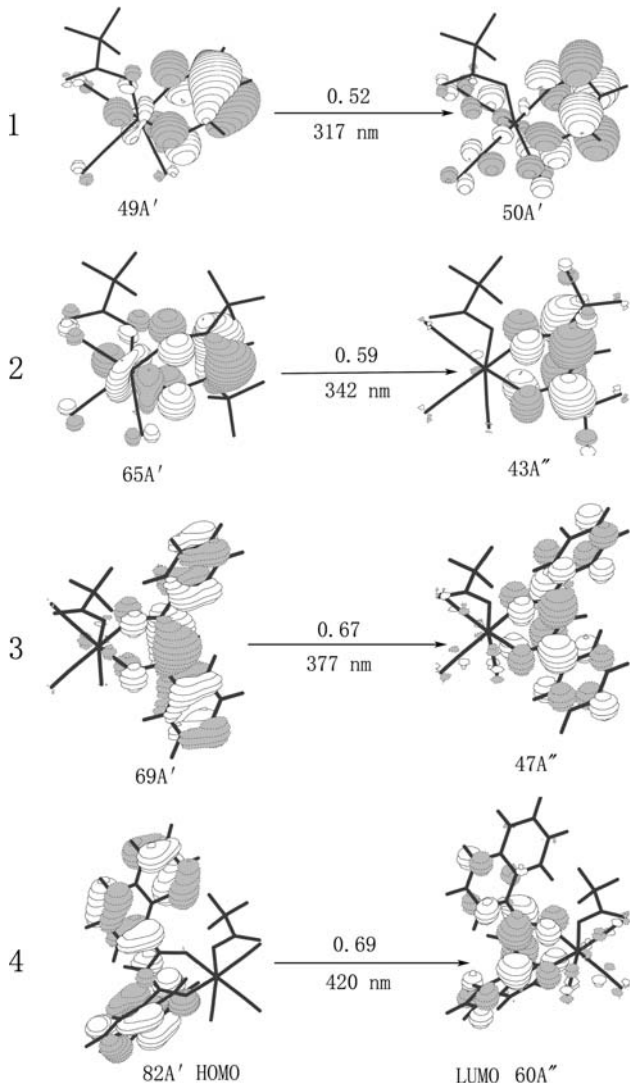

Fig. 4 Single electron transitions with the maximum CI coefficients under TD-DFT calculations for the lowest energy absorptions of four complexes in CH_2Cl_2

transition, which are in accordance with above analysis of molecular orbital composition.

For the third absorption band, the most representative absorption of **1–4** appears at 215 (5.75 eV), 210 (5.88 eV), 245 (5.06 eV), and 256 nm (4.83 eV), respectively. Table 7 shows that the excitation of MO 24a″ → MO 51a′ is the dominant contribution to the absorption of **1** at 215 nm. Table 3 shows that MO 24a″ is mainly composed of 53.5% d(Os), 36.2% π(ctfa), and 10.4% π(acac), while the MO 51a′ is the 17.3% d(Os) and 74.2% π*(ctfa) type orbital, so the absorption can be described as a [d_{xy}(Os) + π(acac) + π(ctfa)] → [d(Os) + π*(ctfa)] transition with MLCT/LLCT character. The absorptions of **2–4** at 210, 245, and 256 nm have similar transition character to that of **1** at 215 nm. It is similar to the second absorption band. Moreover, by electronic density diagrams (Fig. S2) we can further understand the process of excitation.

The UV–vis spectrum of **2** in CH_2Cl_2 shows that the $^1\pi\pi^*/^1$MLCT band is at 336 nm, two stronger absorption bands of **3** are at 367 and 280 nm, which are consistent with calculated absorption bands at 342 nm of **2**, 377 and 284 nm of **3**.

3.3 The emission spectra of **1–4** in the CH_2Cl_2 solution

In the TD-DFT calculations, the phosphorescences of **1–4** are from ^{3}A′ excited state. The calculated phosphorescence and the measured emission in CH_2Cl_2 media are summarized in Table 7. The frontier molecular orbital compositions that are responsible for the emissions are compiled in Table 8. The intuitive electron transition diagram of the emission is shown in Fig. 5.

For the calculated phosphorescence at 444.41 nm (2.79 eV) of **1**, the excitation of MO 27a″ → MO 49a′ has the largest configuration coefficient (0.56) and causes the emission. The orbital analysis reveals that the emission originates from the ^{3}[π(acac) + d_z^2(Os) + π(ctfa) → π*(ctfa) + π*(acac)] transition with ^{3}LLCT/^{3}ILCT/^{3}MLCT character. Figure 5 displays an intuitive electron transition diagram of the emission; we can perceive that the emission is attributed to ππ*/MLCT characters.

The calculated phosphorescences of **2** and **3** are at 521.54 (2.38 eV) and 561.15 nm (2.21 eV), respectively. The emission of **2** at 521 nm arises from $X^3A \rightarrow A^1A'$ transition and the excitation of MO 43a″ → MO 65a′ is the dominant contribution. As seen from Table 8, the MO 43a″ (LUMO) are significantly localized on the acac ligand above 77% compositions, while the MO 65a′ (HOMO) are mainly contributed by Os(II), ctfa, and acac ligands. According to above analysis, the phosphorescence is attributed to the ^{3}[d(Os) + π(acac) + π(ctfa) → π*(acac) + π*(CF_3)] transition with ^{3}LLCT/^{3}LXCT^3/MLCT characters, which is very similar to that of complex **1**, except the slight effect of $-CF_3$ group. The analogous trend has been observed from the absorption spectrum of **2**. From Tables 7 and 8, the phosphorescences at 561 nm of **3** and 525 nm of **4**, originating from the MO 47a″ → MO 69a′ and MO 60a″ → MO 82a′ transition, are essentially attributed to the ^{3}[π(acac) + π(X) → π*(acac) + π*(X)] ^{3}ππ* transition, which are in accordance with their lowest energy absorption in term of transition properties. Experimentally, the measured phosphorescences of **2** and **3** at 545 and 541 nm in CH_2Cl_2 media have been tentatively assigned to a ^{3}ππ*/^{3}MLCT transition. The proportion of MLCT transition is very small, only 11% for **2**. For **3** and **4**, the X substituent compositions increase from 27.8% of **3** to 88.8% of **4** in HOMO, while the metal compositions

Table 8 Molecular orbital compositions (%) in the $^3A'$ excited states for **1–4** at the B3LYP level of theory

	Orbital	Energy(ev)	Composition (%)				Main bond type	Os comp.
			Os	ctfa	acac	X		
1	27a″	−2.1105		43.7	55.6		π*(ctfa) + π*(acac)	
	50a′(L)	−2.3503	12.1	56.0	31.8		d(Os) + π*(ctfa) + π*(acac)	$4.7d_{xy}$
	49a′(H)	−6.8527	19.3	12.6	68.1		d(Os) + π(acac) + π(ctfa)	$11.1d_{z^2}$
	26a″	−7.6840	42.1	54.5			d(Os) + π(ctfa)	$34.1d_{yz}$
2	44a″	−2.4047	12.5	73.8	12.0		d(Os) + π*(ctfa) + π*(acac)	$4.0d_{yz}$
	43a″(L)	−3.3206	3.8		76.8	14.7	π*(acac) + π*(CF_3)	
	65a′(H)	−7.4478	28.2	17.9	52.1		d(Os) + π(acac) + π(ctfa)	$13.6d_{z^2}$
	42a″	−7.8554	38.5	58.9			d(Os) + π(ctfa)	$29.8d_{xz}$
3	70a′	−1.7848	15.6	64.1	15.3		d(Os) + π*(ctfa) + π*(acac)	$5.5d_{z^2}$
	47a″(L)	−2.7364			55.0	34.4	π*(acac) + π*(C_6H_5)	
	69a′(H)	−6.3125			58.0	27.8	d(Os) + π(acac) + π(C_6H_5)	$3.4d_{x^2-y^2}$
	46a″	−7.1724	24.1		21.5	43.7	d(Os) + π(C_6H_5) + π(acac)	$9.6d_{yz} + 8.6d_{xz}$
4	61a″	−1.8561	17.5	60.0	15.7		d(Os) + π*(ctfa) + π*(acac)	$4.2d_{xz} + 3.6d_{xy}$
	60a″(L)	−2.4240			52.5	40.9	π*(acac) + π*($C_{10}H_7$)	
	82a′(H)	−6.0162	0.3		10.7	88.8	π($C_{10}H_7$) + π(acac)	
	59a″	−6.1066			8.2	90.5	π($C_{10}H_7$) + π(acac)	

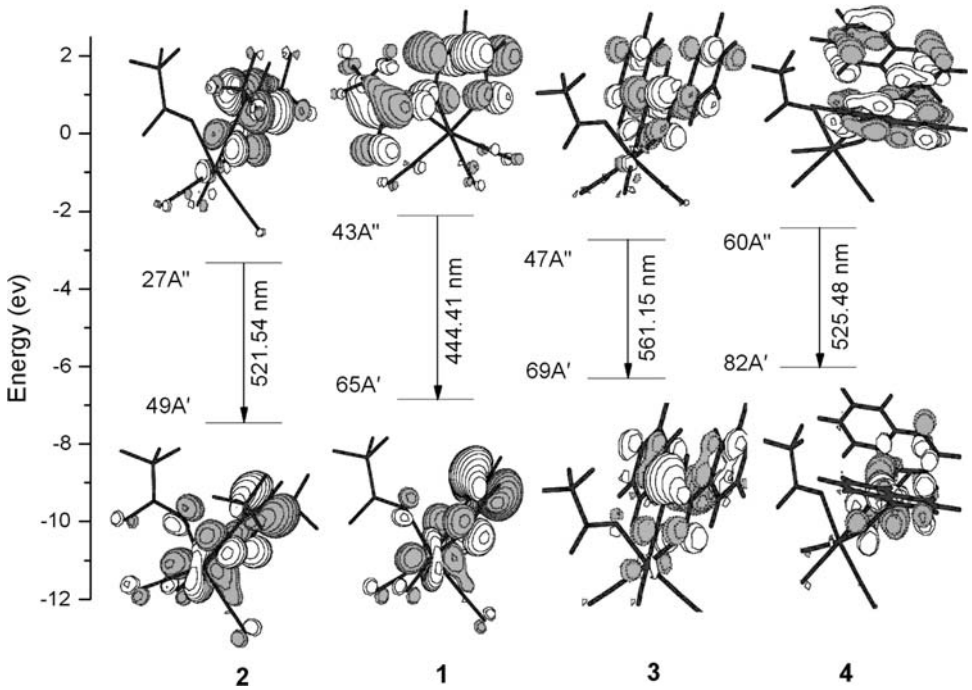

Fig. 5 Transitions responsible for the emissions at 444, 521, 561, and 525 nm for **1–4**, respectively, simulated in CH_2Cl_2

reduce, directly leading to the change of transition properties.

We have presented in the above discussions that the lowest-energy emissions and absorptions have the same transition character for each complexes; the phosphorescent emissions should come from the lowest-energy absorptions. The energy differences between the calculated lowest-energy absorptions and emissions of **1–4** are 1.12, 1.24, 1.07, and 0.59 eV, respectively, as the Stokes shifts the modest shifts, are in agreement with the little change between the ground- and excited-state structures. In addition, the emission of **1–3** is still dominated by phosphorescence, as indicated by its large Stokes-shift; but for **4**, the emission is dominated by phosphorescence and fluorescence, as indicated by its smaller Stokes-shift, and the fluorescence of **4** at 439 nm was also calculated.

Obviously, the phosphorescent excited state is relevant to both the metal and the ligands, and the intense interaction between the metal and the ligands in the frontier molecular orbitals leads to the spin-forbidden LC ($\pi\pi^*$) transition. Many researchers of Ir complexes have speculated that the more metal components in the frontier molecular orbital (HOMO) make the spin-forbidden transition more possible, and it could enhance the quantum efficiencies of complexes [21, 23, 24, 59–65]. In this work, the metal components of **2–3** in the frontier molecular orbital are reduced, but the emission yields increase from **2** (0.05) to **3** (0.13). It indicates that this conjecture is inapplicable for this kind of Os complexes, or it may be suitable to the lowest energy absorptions and the emissions of complexes mainly from the MLCT transition. Further experimental and theoretical studies are needed to consider this problem. At last, we hope that these theoretical studies will assist in the design of highly efficient phosphorescent materials.

Time-dependent density functional theory (TDDFT) has gained widespread use in photochemistry due to its reasonable accuracy and low computational cost. This method has successfully been used in the excited state calculations for a variety of molecular systems [23, 66–69]. However, very recently some studies have also highlighted an underestimation of low-lying TDDFT excitation energies associated with significant charge transfer (CT) [70–72]. Consequently, some of research groups [73, 74] consider correcting TDDFT by using different exchange-correlation functionals, for instance, the newly developed LC–TDDFT method [75]. But, the LC scheme is only used in some small molecular systems via the software program written by "their own administrator". Therefore, in the present work we made use of the TDDFT method to calculate the charge-transfer excitation energy. And the calculated results are in good agreement with the experiment observations.

4 Conclusions

In this paper we investigate the geometry structures and absorption, and phosphorescent properties of four Os(II) β-diketonate monodentate complexes theoretically. The calculated results reveal that the transition properties of **1–4** change from $\pi\pi^*$/MLCT mixing transition to pure $\pi\pi^*$ transition with the increasing of the π electron-donating ability of X substituents; the absorption and emission wavelength of substitution derivatives **(2–4)** are red-shifted compared with that of parent complex **1**. This indicates that the emission color could be adjusted by changing electron-donating ability of the X substituent. Therefore, these β-diketonate complexes can be used to design many luminescent materials.

Acknowledgments This work is supported by the Natural Science Foundation of China (Grant Nos. 20173021, 20333050, and 20573042).

References

1. Balzani V, Juris A, Venturi M, Campagna S, Serroni S (1996) Chem Rev 96:759. doi:10.1021/cr941154y
2. Vlcek A Jr (1998) Coord Chem Rev 177:219. doi:10.1016/S0010-8545(98)00187-8
3. Demadis KD, Hartshorn CM, Meyer TJ (2001) Chem Rev 101:2655. doi:10.1021/cr990413m
4. Demas JN, DeGraff BA (2001) Coord Chem Rev 211:317. doi:10.1016/S0010-8545(00)00278-2
5. Carlson B, Phelan GD, Kaminsky W, Dalton L, Jiang X, Liu S, Jen AKY (2002) J Am Chem Soc 124:14162. doi:10.1021/ja0176705
6. Amarante D, Cherian C, Catapano A, Adams R, Wang MH, Megehee EG (2005) Inorg Chem 44:8804. doi:10.1021/ic051171d
7. Tung YL, Chen LS, Chi Y, Chou PT, Cheng YM, Li EY, Lee GH, Shu CF, Wu FI, Carty AJ (2006) Adv Funct Mater 16:1615. doi:10.1002/adfm.200500901
8. Baldo MA, O'Brien DF, You Y, Shoustikov A, Sibley S, Thompson ME, Forrest SR (1998) Nature 395:151. doi:10.1038/25954
9. Holder E, Langeveld BMW, Schubert US (2005) Adv Mater 17:1109. doi:10.1002/adma.200400284
10. Gong X, Ostrowski JC, Bazan GC, Moses D, Heeger AJ (2002) Appl Phys Lett 81:3711. doi:10.1063/1.1511283
11. Kawamura Y, Goushi K, Brooks J, Brown JJ, Sasabe H, Adachi C (2005) Appl Phys Lett 86:1104. doi:10.1063/1.1862777
12. Adachi C, Baldo MA, Thompson ME, Forrest SR (2001) J Appl Phys 90:5048. doi:10.1063/1.1409582
13. O'Regan B, Grätzel M (1991) Nature 353:737. doi:10.1038/353737a0
14. Szmacinski H, Lakowicz JR (1995) Sens Actuat B 29:16. doi:10.1016/0925-4005(95)01658-9
15. Castellano FN, Lakowicz JR (1998) Photochem Photobiol 67:179. doi:10.1562/0031-8655(1998)067<0179:AWSLOS>2.3.CO;2
16. Lakowicz JR, Castellano FN, Dattelbaum JD, Tolosa L, Rao G, Gryczynski I (1998) Anal Chem 70:5115. doi:10.1021/ac980876c
17. de Silva AP, Gunaratne HQ, Gunnlaugsson T, Huxley AJM, McCoy CPJ, Rademacher T, Rice TE (1997) Chem Rev 97:1515. doi:10.1021/cr960386p
18. Chen YL, Li SW, Chi Y, Cheng YM, Pu SC, Yeh YS, Chou PT (2005) ChemPhysChem 6:2012. doi:10.1002/cphc.200500252
19. Chen YL, Sinha C, Chen IC, Liu KL, Chi Y, Yu JK, Chou PT, Luc TH (2003) Chem Commun, p 3046
20. Su MD, Liao HY, Chu SY, Chi Y, Liu CS, Lee FJ, Peng SM, Lee GH (1998) Organomet 17:3387. doi:10.1021/om980213l
21. Lamansky S, Djurovich P, Murphy D, Abdel-Razzaq F, Kwong R, Tsyba I, Bortz M, Mui B, Bau R, Thompson ME (2001) Inorg Chem 40:1704. doi:10.1021/ic0008969
22. Bruce MI, Liddell MJ, Hughes CA, Skelton BW, White AH (1988) J Organomet Chem 347:157. doi:10.1016/0022-328X(88)80280-8

23. Liu T, Xia BH, Zhou X, Zhang HX, Pan QJ, Gao JS (2007) Organomet 26:143. doi:10.1021/om0606338
24. Lamansky S, Djurovich P, Murphy D, Abdel-Razzaq F, Lee HE, Adachi C, Burrows PE, Forrest SR, Thompson ME (2001) J Am Chem Soc 123:4304. doi:10.1021/ja003693s
25. Stufkens DJ (1992) Comments. Inorg Chem 13:359. doi:10.1080/02603599208048467
26. Zipp AP, Sacksteder L, Streich J, Cook A, Demas JN, DeGraff BA (1993) Inorg Chem 32:5629. doi:10.1021/ic00076a035
27. Sacksteder L, Lee M, Demas JN, DeGraff BA (1993) J Am Chem Soc 115:8230. doi:10.1021/ja00071a036
28. Rossenaar BD, Stufkens DJ, Vlcek A (1996) Inorg Chem 35:2902. doi:10.1021/ic9509802
29. Yam VWW, Lau VCY, Wu LX (1998) J Chem Soc Dalton Trans, p 1461. doi:10.1039/a801575i
30. Vogler A, Kunkely H (2000) Coord Chem Rev 200:991. doi:10.1016/S0010-8545(99)00241-6
31. Striplin DR, Crosby GA (2001) Coord Chem Rev 211:163. doi:10.1016/S0010-8545(00)00277-0
32. Leininger S, Olenyuk B, Stang PJ (2000) Chem Rev 100:853. doi:10.1021/cr9601324
33. Sun SS, Lees AJ (2002) Organomet 21:39. doi:10.1021/om0106027
34. Woessner SM, Helms JB, Houlis JF, Sullivan BP (1999) Inorg Chem 38:4380. doi:10.1021/ic9812813
35. Yam VWW (2001) Chem Commun (Camb) 789. doi:10.1039/b006694j
36. Chi Y, Lan JW, Peng SM, Lee GH (2001) J Cluster Sci 12:2. doi:10.1023/A:1016625218456
37. Su MD, Liao HY, Chu SY, Chi Y, Liu CS, Lee FJ, Peng SM, Lee GH (2000) Organomet 19:5400. doi:10.1021/om000537l
38. Runge E, Gross EKU (1984) Phys Rev Lett 52:997. doi:10.1103/PhysRevLett.52.997
39. Becke AD (1993) J Chem Phys 98:5648. doi:10.1063/1.464913
40. Stanton JF, Gauss J, Ishikawa N, Head-Gordon MJ (1995) Chem Phys 103:4160. doi:10.1063/1.469601
41. Foreman JB, Head-Gordon M, Pople A (1992) J Phys Chem 96:135. doi:10.1021/j100180a030
42. Waiters VA, Hadad CM, Thiel Y, Colson SD, Wibergy KB, Johnson PM, Foresmanl JB (1991) J Am Chem Soc 113:4782. doi:10.1021/ja00013a011
43. Zhang HX, Che CM (2001) Chem Eur J 7:4887. doi:10.1002/1521-3765(20011119)7:22<4887::AID-CHEM4887>3.0.CO;2-C
44. Pan QJ, Zhang HX (2003) J Chem Phys 119:4346. doi:10.1063/1.1592493
45. Pan QJ, Zhang HX (2004) J Phys Chem A 108:3650. doi:10.1021/jp049873w
46. Pan QJ, Zhang HX (2003) Eur J Inorg Chem 4202. doi:10.1002/ejic.200300389
47. Pan QJ, Zhang HX (2004) Inorg Chem 43:593. doi:10.1021/ic0300159
48. Casida ME, Jamorski C, Casida KC, Salahub DR (1998) J Chem Phys 108:4439. doi:10.1063/1.475855
49. Stratmann RE, Scuseria GE (1998) J Chem Phys 109:8218. doi:10.1063/1.477483
50. Matsuzawa NN, Ishitani A (2001) J Phys Chem A 105:4953. doi:10.1021/jp003937v
51. Cossi M, Scalmani G, Regar N, Barone V (2002) J Chem Phys 117:43. doi:10.1063/1.1480445
52. Barone V, Cossi M (1997) J Chem Phys 107:3210. doi:10.1063/1.474671
53. Monat JE, Rodriguez JH, McCusker JK (2002) J Phys Chem A 106:7399. doi:10.1021/jp020927g
54. Yang L, Feng JK, Ren AM (2005) Synth Met 152:265. doi:10.1016/j.synthmet.2005.07.091
55. Wadt WRP (1985) J Chem Phys 82:284. doi:10.1063/1.448800
56. Hay PJ, Hay WR (1985) J Chem Phys 82:299. doi:10.1063/1.448975
57. Frisch MJ, Trucks GW, Schlegel HB, Scuseria GE, Robb MA, Cheeseman JR, Montgomery JA Jr, Vreven T, Kudin KN, Burant JC, Millam JM, Iyengar SS, Tomasi J, Barone V, Mennucci B, Cossi M, Scalmani G, Rega N, Petersson GA, Nakatsuji H, Hada M, Ehara M, Toyota K, Fukuda R, Hasegawa J shida M, Nakajima T, Honda Y, Kitao O, Nakai H, Klene M, Li, Knox JE, Hratchian HP, Cross JB, Bakken V, Adamo C, jaramillo J, Gomperts R, Stratmann R E, Yazyev O, Austin AJ, Cammi R, Pomelli C, Ochterski JW, Ayala PY, Morokuma K, Voth GA, Salvador P, Dannenberg JJ, Zakrzewski VG, Dapprich S, Daniels AD, Strain MC, Farkas O, Malick DK, Rabuck AD, Raghavachari K, Foresman JB, Ortiz JV, Cui Q, Baboul AG, Clifford S, Cioslowski J, Stefanov BB, Liu G, Liashenko A, Piskorz P, Komaromi I, Martin RL, Fox DJ, Keith T, Al-Laham MA, Peng CY, Nanayakkara A, Challacombe M, Gill, PMW, Johnson B, Chen W, Wong MW, Gonzalez C, Pople JA (2004) Gaussian 03, revision C.02. Gaussian, Inc.: Wallingford, CT, USA
58. Shapley PA, Marshman RM, Shusta JM, Gebeyehu Z, Wilson SR (1994) Inorg Chem 33:498. doi:10.1021/ic00081a017
59. Doedens RJ, Ibers JA (1967) Inorg Chem 6:204. doi:10.1021/ic50048a004
60. Zhang YH, Xia BH, Pan QJ, Zhang HX (2006) J Chem Phys 124:144309. doi:10.1063/1.2189220
61. Hay PJ (2002) J Phys Chem A 106:1634. doi:10.1021/jp013949w
62. Markham JPJ, Lo SC, Magennis SW, Burn PL, Samuel IDW (2002) Appl Phys Lett 80:2645. doi:10.1063/1.1469218
63. Adachi C, Baldo MA, Forrest SR (2000) Appl Phys Lett 77:904. doi:10.1063/1.1306639
64. Colombo MG, Gudel HU (1993) Inorg Chem 32:3081. doi:10.1021/ic00066a019
65. Baldo MA, Lamansky S, Burrows PE, Thompson ME, Forrest SR (1999) Appl Phys Lett 75:4. doi:10.1063/1.124258
66. Jamorski C, Foresman JB, Thilgen C, Lüthi HP (2002) J Chem Phys 116:8761. doi:10.1063/1.1465404
67. Rappoport D, Furche F (2004) J Am Chem Soc 126:1277. doi:10.1021/ja037806u
68. Jacquemin D, Bouhy M, Perpète EA (2006) J Chem Phys 124:204321. doi:10.1063/1.2202735
69. Nemykin VN, Makarova EA, Grosland JO, Hadt RG, Koposov AY (2007) Inorg Chem 46:9591. doi:10.1021/ic700558v
70. Fabian J (2001) Theor Chem Acc 106:199. doi:10.1007/s002140100250
71. Liao MS, Lu Y, Scheiner S (2003) J Comput Chem 24:623. doi:10.1002/jcc.10226
72. Dreuw A, Head-Gordon M (2004) J Am Chem Soc 126:4007. doi:10.1021/ja039556n
73. Neugebauer J, Gritsenk O, Baerends EJ (2006) J Chem Phys 124:214102. doi:10.1063/1.2197829
74. Chiba M, Tsuneda T, Hirao K (2006) J Chem Phys 124:144106. doi:10.1063/1.2186995
75. Tawada Y, Tsuneda Ta, Yanagisawa S, Yanai T, Hirao K (2004) J Chem Phys 120:8425. doi:10.1063/1.1688752